CrystEngComm

PAPER

View Article Online
View Journal | View Issue

Cite this: *CrystEngComm*, 2014, **16**, 252

Syntheses, structures and properties of two multi-iron–samarium/multi-iron substituted germanotungstates†

Jun Wang,[a] Jun-Wei Zhao,*[b] Hai-Yan Zhao,[a] Bai-Feng Yang,[a] Huan He[a] and Guo-Yu Yang*[ac]

Received 7th October 2013,
Accepted 4th November 2013

DOI: 10.1039/c3ce42023j

www.rsc.org/crystengcomm

A heterometallic hexameric germanotungstate containing iron–lanthanide cluster fragments $(enH_2)_{13}HK_9[Fe_6Sm_6(H_2O)_{12}(\alpha\text{-}GeW_{10}O_{38})_6]\cdot 42H_2O$ (**1**) and a hexairon substituted double sandwich-type germanotungstate $(enH_2)_6K[HFe_6(B\text{-}\alpha\text{-}GeW_9O_{34})_2(\alpha\text{-}GeW_6O_{26})(H_2O)_2]\cdot 11H_2O$ (**2**) (en = 1,2-ethylenediamine) have been hydrothermally synthesized and structurally characterized using elemental analyses, inductively coupled plasma atomic emission spectrometry, IR spectra, powder X-ray diffraction (PXRD), thermogravimetric (TG) analyses and single-crystal X-ray diffraction. The common features of **1** and **2** are that both are based on lacunary Keggin-type germanotungstate fragments. **1** is the first heterometallic hexameric germanotungstate consisting of six {Fe–(μ_3-O)$_3$–Sm} bridges, while two double sandwich-type fragments in **2** are connected together through two potassium cations forming hexameric germanotungstate units. The magnetic susceptibility measurements demonstrate the presence of antiferromagnetic interactions in both compounds.

Introduction

Polyoxometalates (POMs), as a rapidly growing class of metal–oxygen clusters with versatile structural topologies, oxygen-enriched surfaces and interesting properties, are excellent candidates for making novel larger aggregates with potential applications in catalysis, materials science and medicine.[1–8] Notably, transition-metal-substituted POMs (TMSPs) constitute one of the most exciting developments in POM chemistry in the past several decades.[9–13] A vast variety of TMSPs have been made using conventional aqueous solution methods. However, it is noteworthy that Yang's group put forward an innovative synthetic strategy in 2007, lacunary directing syntheses *via* the lacunary sites of POM fragments were applied under hydrothermal conditions to make novel TMSPs by combining lacunary POM precursors, TM cations and organoamines in a given system.[14] Compared to the conventional aqueous solution method, the hydrothermal technique opened a new window for making unprecedented TMSPs.[15]

On the one hand, TMSPs are of particular interest due to their magnetic properties.[16,17] From the magnetism point of view, incorporation of much more spin-coupled paramagnetic TM ions into lacunary POM lattices may result in molecule-based materials with high-spin ground states, large spin anisotropies, hysteresis, *etc.*[18] Moreover, the chemistry of d-electron TMSPs continues to attract much interest in redox- and acid-dependent catalysis, medicinal and materials applications.[19] Among d-electron TMSPs, iron-substituted POMs are interesting for catalytic applications involving the easily accessible Fe^{2+}/Fe^{3+} redox couple and magnetic applications due to the large number of unpaired electrons in high-spin $Fe^{2+/3+}$ combined with the possibility of forming spin-crossover molecular magnetic materials.[20] So far, some iron-containing POMs have been reported. For example, in 2006–2007, Hill *et al.* addressed several dilacunary multi-Fe^{III} substituted γ-Keggin silicotungstates, $[\{Fe_2(OH)_3(H_2O)_2\}_3(\gamma\text{-}SiW_{10}O_{36})_3]^{15-}$,[21a] $[\{Fe(OH)(OAc)\}_4(\gamma\text{-}SiW_{10}O_{36})_2]^{12-}$,[21b] and $[\{Fe_6(OH)_9(H_2O)_2(OAc)_2\}(\gamma\text{-}SiW_{10}O_{36})_3]^{17-}$,[21b] and evaluated the former catalytic aerobic oxidation activity.[21a] In 2007, Yang *et al.* reported a mixed-valence-iron-containing tetramer $[\{Fe^{II}_{1.5}Fe^{III}_{12}(\mu_3\text{-}OH)_{12}(\mu_4\text{-}PO_4)_4\}(B\text{-}\alpha\text{-}PW_9O_{34})_4]^{18-}$.[14b] Kortz *et al.* made two unusual Fe-substituted germanotungstates (GTs) $[K(H_2O)(\beta\text{-}Fe_2GeW_{10}O_{37}(OH))(\gamma\text{-}GeW_{10}O_{36})]^{12-}$ and $[\{\beta\text{-}Fe_2GeW_{10}O_{37}(OH)_2\}_2]^{12-}$.[22] Cronin *et al.* addressed a Fe^{III}-substituted tetrahedral anion $[KFe_{12}(OH)_{18}(\alpha\text{-}P_2W_{15}O_{56})_4]^{29-}$.[23] Sécheresse *et al.* reported a tetrahedral Fe_{13}

[a] *DOE Key Laboratory of Cluster Science, School of Chemistry, Beijing Institute of Technology, Beijing 100081, China. E-mail: ygy@bit.edu.cn*
[b] *Henan Key Laboratory of Polyoxometalate Chemistry, College of Chemistry and Chemical Engineering, Henan University, Henan 475004, Kaifeng, China. E-mail: zhaojunwei@henu.edu.cn*
[c] *State Key Laboratory of Structural Chemistry, Fujian Institute of Research on the Structure of Matter, Chinese Academy of Sciences, Fuzhou, Fujian 350002, China. E-mail: ygy@fjirsm.ac.cn; Fax: +86 591 8371 0051*

† Electronic supplementary information (ESI) available: The X-ray crystallographic files for **1** and **2** in CIF format, IR spectra, XRPD patterns and the additional structural figures of **1** and **2**. CCDC 961135 and 961136 for **1** and **2**, respectively. For ESI and crystallographic data in CIF or other electronic format see DOI: 10.1039/c3ce42023j

substituted anion $[\{(B\text{-}\alpha\text{-}PW_9O_{34})Fe_3(OH)_3\}_4(PO_4)_4Fe]^{22-}$.[24] In 2008, Sécheresse *et al.* made four sandwich-type TMSPs, $[Fe^{III}_4(H_2O)_8(SbW_9O_{33})_2]^{6-}$, $[Fe^{III}_4(ox)_4(H_2O)_2(SbW_9O_{33})_2]^{14-}$, $[Fe^{III}_4(ox)_4(SbW_9O_{33})_2]^{14-}$ and $[Fe^{II}_2Fe^{III}_2(enH)_2(Fe^{III}W_9O_{34})_2]^{10-}$.[25] In 2009, Yang *et al.* obtained a banana-shaped anion $[Fe_6Ge_3W_{24}O_{94}(H_2O)_2]^{14-}$.[26] In 2010, Wang *et al.* discovered {WFe_9} incorporated cluster $[WFe_9(\mu_3\text{-}O)_3(\mu_2\text{-}OH)_6O_4H_2O(SiW_9O_{34})_3]^{9-}$.[27] In 2011, Zhao *et al.* reported an S-shaped multi-iron substituted arsenotungstate $\{[(\alpha\text{-}H_2AsW_6O_{26})Fe_3(H_2O)(B\text{-}\alpha\text{-}H_4AsW_9O_{34})]_2[Fe]_2\}^{4-}$.[8]

On the other hand, recently, more and more advances in the synthesis of paramagnetic metal aggregates have been focused on the design and synthesis of POM-based TM–Ln (Ln = lanthanide) heterometallic systems attributed to their exploitable applications in magnetism, bimetallic catalysis and molecular adsorption as well as their intriguing architectures and topologies.[28–31] However, the simultaneous reactions of lacunary POM precursors with TM and Ln cations are comparatively difficult in the same system because of the occurrence of unavoidable competitive reactions among highly negative POM precursors, strongly oxyphilic Ln cations and less active TM cations in the reaction system. The oxyphilic Ln cations usually possess high reactivity with polyanions, which always leads to precipitation instead of crystallization.[32] Therefore, it is still difficult to prepare TM–Ln heterometallic POMs. In 2008, Wang *et al.* reported a POM-based Fe–Ce heterometallic aggregate $[HMTA\text{-}CH_3]_2K_{3.5}Na_{8.5}[K\subset\{FeCe(AsW_{10}O_{38})(H_2O)_2\}_3]\cdot\sim36H_2O$ (HMTA-CH_3 = methyl-hexamethylenetetraamine) with three {α-AsW_{10}} units bridged by three {Fe–O_3–Ce} heterometallic clusters.[30c] In 2011, they discovered another two Fe–Ln hexameric silicotungstates, $(H_2en)_6Na_{15}K_9[Dy_6Fe_6(H_2O)_{12}(SiW_{10}O_{38})_6]\cdot34H_2O$ and $K_{13}Na_{17}[H_2en]_3[Tb_6Fe_6(H_2O)_{12}(SiW_{10}O_{38})_6]\cdot40H_2O$, which were decorated by six {Ln–(μ_3-O)$_3$–Fe} heterometallic clusters.[33] In 2012, Zhao *et al.* made a series of Cu^{II}–Ln^{III} heterometallic GTs, which were mainly constructed by two kinds of backbones, $\{[Cu_3Ln(en)_3(OH)_3(H_2O)_2](\alpha\text{-}GeW_{11}O_{39})\}^{24-}$ and $\{Cu(en)_2[Ln(\alpha\text{-}GeW_{11}O_{39})_2]_2\}^{24-}$.[32c] However, it is worth mentioning that they used the trivacant $[A\text{-}\alpha\text{-}GeW_9O_{34}]^{10-}$ precursor and obtained the monovacant $[\alpha\text{-}GeW_{11}O_{39}]^{8-}$ GTs. In this paper, we also used the trivacant $[A\text{-}\alpha\text{-}GeW_9O_{34}]^{10-}$ precursor to react with $FeSO_4\cdot7H_2O$ and $Sm(NO_3)\cdot6H_2O$ in the presence of en under hydrothermal conditions and obtained a heterometallic hexameric GT containing Fe–Sm clusters $(enH_2)_{13}HK_9[Fe_6Sm_6(H_2O)_{12}(\alpha\text{-}GeW_{10}O_{38})_6]\cdot42H_2O$ (**1**) and a hexa-Fe substituted double sandwich-type GT $(enH_2)_6K[HFe_6(B\text{-}\alpha\text{-}GeW_9O_{34})_2(\alpha\text{-}GeW_6O_{26})(H_2O)_2]\cdot11H_2O$ (**2**). Unexpectedly, there is no Sm in the structure of **2**. It should be noted that **1** and **2** consist of di-, tri- or hexavacant Keggin GT fragments, which are obviously different from the monovacant Keggin fragments observed in the reported Cu^{II}–Ln^{III} heterometallic germanotungstates.[32c] **1** is the first heterometallic hexameric GT consisting of six {Fe–(μ_3-O)$_3$–Sm} bridges, while two double sandwich-type fragments in **2** are connected together through two potassium cations forming hexameric GT units. Magnetic susceptibility measurements of **1** and **2** show the antiferromagnetic interactions with the magnetic centers.

Experimental section

Materials and general methods

All chemical reagents were commercially purchased without further purification. $K_8Na_2[A\text{-}\alpha\text{-}GeW_9O_{34}]\cdot25H_2O$ was made according to the literature[34] and characterized using IR spectra. Elemental analyses (C, H and N) were performed using a Euro EA 3000 CHNS/O analyzer. Inductively coupled plasma atomic emission spectrometry analyses were performed using a Jobin Yvon Ultima 2 spectrometer. IR spectra were obtained from a solid sample pelletized with KBr on a Smart Omni-Transmission spectrometer in the range 400–4000 cm^{-1}. PXRD measurements were performed using a Bruker D8 Advance XRD diffractometer with Cu Kα radiation (λ = 1.54056 Å). TG measurements were taken under a flowing air atmosphere on a Mettler TGA/SDTA 851 thermal instrument with a heating rate of 10 °C min^{-1} from 25 to 800 °C. Magnetic measurements were carried out with a Quantum Design MPMS XL–5 SQUID magnetometer in the temperature range of 2–300 K. The susceptibility data were corrected from the diamagnetic contributions as deduced by using Pascal's constant tables.

Synthesis of $(enH_2)_{13}HK_9[Fe_6Sm_6(H_2O)_{12}(\alpha\text{-}GeW_{10}O_{38})_6]\cdot42H_2O$ (1)

A mixture of $K_8Na_2[A\text{-}\alpha\text{-}GeW_9O_{34}]\cdot25H_2O$ (0.300 g, 0.10 mmol), $FeSO_4\cdot7H_2O$ (0.083 g, 0.30 mmol), $Sm(NO_3)_3\cdot6H_2O$ (0.044 g, 0.10 mmol), en (0.05 mL, 0.75 mmol) and 5 mL of distilled water was stirred for 1 h. Then, the pH value of this system was adjusted to 5 with glacial acetic acid. After stirring for 0.5 h, the color of the mixture changed from grey to earth yellow and then this mixture was sealed in a 25 mL Teflon-lined stainless steel autoclave, kept at 160 °C for 5 days and then cooled to room temperature. Yellow prismatic crystals were obtained by filtering, washed with distilled water and dried in air at ambient temperature. Yield: *ca.* 21% (based on $K_8Na_2[A\text{-}\alpha\text{-}GeW_9O_{34}]\cdot25H_2O$). Anal. calcd (%) for $C_{26}H_{239}N_{26}O_{282}K_9Fe_6Sm_6Ge_6W_{60}$: C, 1.69; H, 1.30; N, 1.97; K, 1.90; Fe, 1.81; Ge, 2.36; Sm, 4.88; W, 59.67. Found: C, 1.86; H, 1.56; N, 1.90; K, 2.08; Fe, 1.65; Ge, 2.49; Sm, 4.75; W, 59.90. IR (KBr pellets, cm^{-1}): 3443(vs), 3124(w), 3026(w), 2927(w), 1620(m), 1492(w), 1458(w), 1399(w), 1367(w), 1041(w), 938(s), 869(s), 788(s), 651(s) (Fig. S1†).

Synthesis of $(enH_2)_6K[HFe_6(B\text{-}\alpha\text{-}GeW_9O_{34})_2(\alpha\text{-}GeW_6O_{26})(H_2O)_2]\cdot11H_2O$ (2)

$K_8Na_2[A\text{-}\alpha\text{-}GeW_9O_{34}]\cdot25H_2O$ (0.25 g, 0.08 mmol) was added into 3 mL of distilled water with vigorous stirring (solution A). Then, a mixture of $FeSO_4\cdot7H_2O$ (0.083 g, 0.30 mmol), $Sm(NO_3)_3\cdot6H_2O$ (0.044 g, 0.10 mmol) and 2 mL of distilled water was stirred for 0.5 hour resulting in solution B. In the next step, 1 mL of solution B was dropwise added into solution A. At this point, the color of the mixture was bright yellow. Then, 0.05 mL of en was added into the mixture with vigorous stirring. Three hours later, the pH value of this system was adjusted to 6.5 with glacial acetic acid. After

stirring for 0.5 h, the color of the mixture changed to dark yellow and the mixture was sealed in a 25 mL Teflon-lined stainless steel autoclave, kept at 160 °C for 5 days and then cooled to room temperature. Dark brown crystals were gathered by filtering, washed with distilled water and dried in air at ambient temperature. Yield: *ca.* 12.5% (based on K_8Na_2[A-α-GeW_9O_{34}]·$25H_2O$). Anal. calcd (%) for $C_{12}H_{87}N_{12}O_{107}KFe_6Ge_3W_{24}$: C, 2.03; H, 1.23; N, 2.36; K, 0.55; Fe, 4.71; Ge, 3.06; W, 62.00. Found: C, 2.20; H, 1.37; N, 2.25; K, 0.75; Fe, 4.88; Ge, 2.92; W, 62.38. IR (KBr pellets, cm^{-1}): 3451(vs), 3125(w), 3028(w), 2927(w), 1617(m), 1507(w), 1386(w), 1327(w), 1046(w), 945(s), 869(s), 784(s), 682(s) (Fig. S2†).

Crystallographic data collection and refinements

Intensity data for **1** and **2** were performed using a Gemini A Ultra diffractometer with graphite-monochromated Mo Kα (λ = 0.71073 Å) at 293(2) K. Both structures were solved using the direct method and refined on F^2 by full-matrix least-squares methods using the SHELX 97 program package.[35] Routine Lorentz polarization corrections and empirical absorption correction were applied to intensity data. No hydrogen atoms associated with water molecules were located from the difference Fourier map. Hydrogen atoms attached to carbon and nitrogen atoms were geometrically placed. All hydrogen atoms were refined isotropically as a riding mode using the default SHELXTL parameters. The crystal structures of **1** and **2** contain very large accessible voids. In the refinements, 9 K^+ ions, 3 diprotonated en and 19 water molecules were found from the Fourier maps of **1**, and 1 K^+, 1 diprotonated en and 7 water molecules were found from the Fourier maps of **2**. However, there are still very large accessible solvent voids in their crystal structures, indicating that some more counter cations and water molecules should exist in the structure, but cannot be found from the weak residual electron peaks. Based on the charge-balance considerations, elemental analyses and TG analyses, another 7 diprotonated en molecules were included in the molecular formula of **1**, and another 5 diprotonated en and 3 water molecules were included in the molecular formula of **2** directly. Crystallographic data and structure refinements for **1** and **2** are summarized in Table 1.

Table 1 Crystallographic data and structural refinements for **1** and **2**

	1	**2**
Formula	$C_{26}H_{239}N_{26}O_{282}K_9Fe_6Sm_6Ge_6W_{60}$	$C_{12}H_{87}N_{12}O_{107}KFe_6Ge_3W_{24}$
M_r (g mol^{-1})	18 485.07	7116.31
Crystal system	Monoclinic	Monoclinic
Space group	$C2/c$	$P2_1/n$
a (Å)	20.8479(5)	20.7644(4)
b (Å)	35.6759(9)	25.0049(6)
c (Å)	38.2974(8)	22.6513(5)
β (°)	92.107(2)	100.729(2)
V ($Å^3$)	28 465.1(12)	11 555.2(4)
Z	4	4
D_c (g cm^{-3})	4.313	4.091
μ (mm^{-1})	26.519	25.423
Limiting indices	$-24 \le h \le 24$ $-42 \le k \le 38$ $-37 \le l \le 45$	$-24 \le h \le 24$ $-22 \le k \le 29$ $-26 \le l \le 26$
Measured reflections	70 276	68 378
Independent reflections	24 946	20 162
R_{int}	0.0609	0.0654
Data/restrains/parameters	24 946/95/1660	20 162/108/1252
Goodness-of-fit on F^2	1.069	1.071
R_1, wR_2 [$I > 2\sigma(I)$][a]	0.0491, 0.1024	0.0667, 0.1660
R_1, wR_2 [all data][a]	0.0795, 0.1127	0.1123, 0.1867

[a] $R_1 = R||F_0| - |F_c||/\sum|F_0|$; $wR_2 = \sum[w(F_0^2 - F_c^2)^2]/\sum[w(F_0^2)^2]]^{1/2}$.

Results and discussion

Synthesis

In the initial exploring period, we were particularly interested in Fe–Ln substituted POMs because of their diverse coordination modes, which are very useful in catalytic and magnetic areas. From the viewpoint of lacunary POM fragments, the trivacant Keggin [A-α-GeW_9O_{34}]$^{10-}$ precursor possesses high reaction activity and stability. We chose Fe^{2+}, Sm^{3+} cations and the trivacant Keggin [A-α-GeW_9O_{34}]$^{10-}$ precursor as our reaction system, aiming to make high dimensional Fe–Ln heterometallic clusters. Fortunately, we obtained **1** and **2**. We have studied the influence of synthetic parameters on these two obtained compounds in the following three points: (a) reactant materials: **1** and **2** were both obtained with the same kind of materials but with different usage and adding sequence. In the preparation of **1**, after the mixture of K_8Na_2[A-α-GeW_9O_{34}]·$25H_2O$, $FeSO_4·7H_2O$ and $Sm(NO_3)_3·6H_2O$ in the distilled water at pH = 5 was stirred for 0.5 h, the color turned from grey to earth yellow with lots of precipitates. However, during the synthesis of **2**, after solution B is dropwise added to solution A, the pH value of this system was adjusted to 6.5 with glacial acetic acid and the color of the system turned slowly from bright yellow to dark yellow with the amount of precipitates less than those in **1**. A close inspection of the synthetic conditions of **1** and **2** reveals that the usage of $FeSO_4·7H_2O$ and $Sm(NO_3)_3·6H_2O$ is twice as high for **1** as for **2**; moreover, the reaction activity of the Sm^{3+} cation often is lower than that of the iron cation; therefore, these two main factors can lead to no Sm^{III} element in the structure of **2**. In addition, the discrepancy between pH values of reaction systems and the addition sequence of reactants may also influence the combination between different components and further affect the structural construction. Due to the absence of Sm^{III} element in the structure of **2**, the comparative experiment where $Sm(NO_3)_3·6H_2O$ was removed from the system has been performed, and the result shows that **2** can also be obtained but the yield is very low, and the specific reasons are under investigation. (b) pH values: **1** and **2** are only obtained in the limited pH domain, which are around 5 and 6.5, respectively. At a higher or lower pH value, the yield and the quality of single crystals are decreased. (c) Temperatures: we have tried to obtain **1** and **2** with the reaction temperatures at 120, 140, 160 and 170 °C and found that they could only be isolated when the reaction temperature was set to 160 °C. In a word, the relationships among the three synthetic parameters of reactant materials, pH values

and temperatures are mutually interrelated and interacting with each other.

Structure descriptions of 1 and 2

The good agreements of the PXRD patterns of the bulk of **1** and **2** with the calculated patterns from the single-crystal structural analyses suggest good phase purity of the products (Fig. S3 and S4†). The intensity differences between experimental and simulated PXRD patterns are due to the variation in preferred orientation of the powder samples during collection of the experimental PXRD.

Single-crystal X-ray structural analysis reveals that **1** crystallizes in the monoclinic space group *C*2/*c*. The asymmetric unit of **1** is a trimeric cryptand-type $[KFe_3Sm_3(H_2O)_6(\alpha\text{-}GeW_{10}O_{38})_3]^{17-}$ aggregate that contains three divacant Keggin $[\alpha\text{-}GeW_{10}O_{38}]^{12-}$ subunits, three Sm^{3+} cations, three Fe^{3+} cations and a K^+ cation ($K1^+$). Three $[\alpha\text{-}GeW_{10}O_{38}]^{12-}$ subunits are connected with each other by three [Sm–(μ_3-O)$_3$–Fe] connectors (Fig. 1a). Bond valence sum (BVS) calculations[36] of **1** indicate that the oxidation states of all Fe and Sm atoms are +3 (Table S1†). Among GTs, the commonly employed lacunary GT precursors chiefly include (a) the monovacant $[\alpha\text{-}GeW_{11}O_{39}]^{8-}$, (b) the divacant $[\gamma\text{-}GeW_{10}O_{36}]^{8-}$ and (c) the trivacant $[\alpha\text{-}GeW_9O_{34}]^{10-}$. However, there is no report on the divacant $[\alpha\text{-}GeW_{10}O_{38}]^{12-}$ fragment. In the structure of **1**, we first observe the divacant $[\alpha\text{-}GeW_{10}O_{38}]^{12-}$ fragment. The $Sm1^{3+}$ cation resides in one of the vacant sites of the $[\alpha\text{-}GeW_{10}O_{38}]^{12-}$ unit and exhibits an eight-coordinate distorted square antiprismatic geometry defined by six O atoms from the $[\alpha\text{-}GeW_{10}O_{38}]^{12-}$ units [Sm–O: 2.332(11)–2.878(11) Å] and two water (O114, O115) ligands [Sm–O: 2.505(12)–2.596(13) Å] (Fig. 1b). The coordination spheres of $Sm2^{3+}$ and $Sm3^{3+}$ cations are illustrated in Fig. S5 and S6,† respectively. The $Fe1^{3+}$ cation is incorporated to the other vacant site of the $[\alpha\text{-}GeW_{10}O_{38}]^{12-}$ unit that the $Sm1^{3+}$ cation resides in and shows a six-coordinate octahedral geometry constituted by six O atoms from the $[\alpha\text{-}GeW_{10}O_{38}]^{12-}$ units [Fe–O: 1.926(11)–2.094(12) Å] (Fig. 1c). The coordination geometries of $Fe2^{3+}$ and $Fe3^{3+}$ cations are similar to that of the $Fe1^{3+}$ cation and are not discussed here. Moreover, $Fe1^{3+}$ and $Sm3^{3+}$ cations located in the vacant sites of two adjacent divacant $[\alpha\text{-}GeW_{10}O_{38}]^{12-}$ units are bridged through the μ_3-O groups (O9, O14, O76) forming the unique [Sm–(μ_3-O)$_3$–Fe] unit (Fig. 1d). Particularly, the $K1^+$ ion is encapsulated in the center of the cryptand-type aggregate to enhance its stability and has nine coordinate oxygen atoms. All the coordinate O atoms can be divided into three groups: (O2, O9, O13), (O32, O36, O46), and (O77, O82, O90). Three groups of O atoms are provided correspondingly by three interconnected $[\alpha\text{-}GeW_{10}O_{38}]^{12-}$ units [K–O: 2.777(12)–3.126(12) Å]. Interestingly, the $K1^+$ and nine coordinate O atoms are combined together, forming a beautiful crown-like geometry (Fig. 1e). What's more, two trimeric asymmetric $[Fe_3Sm_3(H_2O)_6(\alpha\text{-}GeW_{10}O_{38})_3]^{18-}$ units are further linked through five K^+ (one $K2^+$, two $K4^+$ and two $K5^+$) ions generating the hexameric structural unit $[K_7Fe_6Sm_6(H_2O)_{12}(\alpha\text{-}GeW_{10}O_{38})_6]^{29-}$ (Fig. 1f).

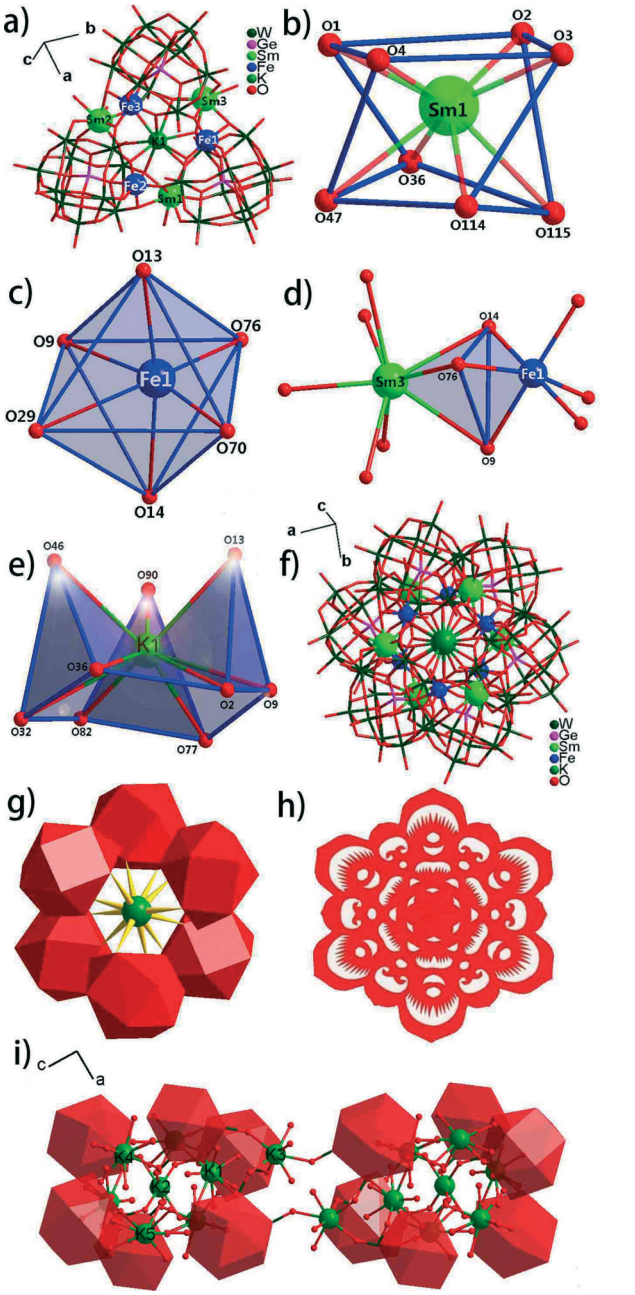

Fig. 1 (a) Ball-and-stick representation of asymmetric unit of **1**. (b) The square antiprismatic coordination geometry around the $Sm1^{3+}$ cation. (c) The eight-coordinate octahedral geometry around the $Fe1^{3+}$ cation. (d) The heterometallic {Fe–(μ_3-O)$_3$–Sm} moiety. (e) The nine-coordinate crown-like geometry around the $K1^+$ cation. (f) Ball-and-stick representation of the hexameric polyoxoanion. (g) Polyhedral view of the hexameric polyoxoanion. (h) A picture of the paper-cut window grilles with a unique Chinese style. (i) The 1-D chain structure of **1**.

The $K2^+$ cation exhibits a six-coordinate octahedral geometry. Two trimeric asymmetric $[Fe_3Sm_3(H_2O)_6(\alpha\text{-}GeW_{10}O_{38})_3]^{18-}$ units are anchored together by $K2^+$ *via* two groups of the same O atoms: (O40, O41, O81) [K–O: 2.622(13)–2.807(12) Å] (Fig. S7†). The $K4^+$ cation has a nine-coordinate geometry, in which O5, O7, O8 and O15 atoms are provided by the

$[\alpha\text{-}GeW_{10}O_{38}]^{12-}$ subunit that encapsulates $Sm1^{3+}$ and $Fe1^{3+}$ cations [K–O: 2.815(13)–2.984(12) Å], the O33 and O42 atoms are from the $[\alpha\text{-}GeW_{10}O_{38}]^{12-}$ subunit that encapsulates $Sm2^{3+}$ and $Fe2^{3+}$ cations [K–O: 2.726(14)–2.986(12) Å] and the O116, O117 and O121 atoms are the water ligands [K–O: 2.75(2)–2.949(8) Å] (Fig. S8†). The $K5^{+}$ cation exhibits the distorted anomalous geometry with K–O distances of 2.814(13)–3.233(12) Å (Fig. S9†). The Sm^{3+}, Fe^{3+} and $K1^{+}$ coordination environments are demonstrated in Fig. S10.† Notably, the distribution of six $[\alpha\text{-}GeW_{10}O_{38}]^{12-}$ fragments surrounding the central $K1^{+}$ ion in $[K_9Fe_6Sm_6(H_2O)_{12}(\alpha\text{-}GeW_{10}O_{38})_6]^{29-}$ (Fig. 1g) looks like paper-cut window grilles with a unique Chinese style (Fig. 1h). Moreover, adjacent hexameric aggregates are interconnected with each other *via* two $K3^{+}$ cations, giving rise to the 1-D chain architecture (Fig. 1i). The $K3^{+}$ cation exhibits the seven-coordinate, severely distorted pentagonal bipyramid defined by five oxygen atoms (O19, O92, O20W, O106, O120) on the equatorial plane [K–O: 2.737(17)–2.922(10) Å] and two oxygen atoms (O48, O19W) on two polar sites [K–O: 2.663(13)–2.70(2) Å] (Fig. S11†). Notably, **1** is similar to those reported $(H_2en)_6Na_{15}K_9[Dy_6Fe_6(H_2O)_{12}(SiW_{10}O_{38})_6]\cdot 34H_2O$ (**A**) and $K_{13}Na_{17}[H_2en]_3[Tb_6Fe_6(H_2O)_{12}(SiW_{10}O_{38})_6]\cdot 40H_2O$ (**B**).[33] But some obvious differences exist between them: (a) their starting materials are distinct. During the course of preparing **1**, $K_8Na_2[A\text{-}\alpha\text{-}GeW_9O_{34}]\cdot 25H_2O$, $FeSO_4\cdot 7H_2O$, $Sm(NO_3)_3\cdot 6H_2O$ and glacial acetic acid were used, while $K_8[\beta_2\text{-}SiW_{11}O_{39}]\cdot 14H_2O$, $FeCl_3$, NaCl, Dy_2O_3/Tb_4O_7, nitric acid and K_2CO_3 were utilized in the formation of **A** and **B**; (b) their reaction time is different. The reaction time for **1** is five days, while the reaction time for **A** and **B** is four days.

2 crystallizes in the monoclinic space group $P2_1/n$. The basic building block of **2** is a double sandwich cluster containing two $[B\text{-}\alpha\text{-}GeW_9O_{34}]^{10-}$ subunits and one $[\alpha\text{-}GeW_6O_{26}]^{12-}$ fragment separated by two Fe_3 clusters (Fig. 2a). Bond valence sum (BVS) calculations[36] indicate that the oxidation states of all Fe atoms are +3 in **2** (Table S1†). It should be emphasized that the $[B\text{-}\alpha\text{-}GeW_9O_{34}]^{10-}$ and $[\alpha\text{-}GeW_6O_{26}]^{12-}$ fragments in **2** are from the isomerization and degradation of the $[A\text{-}\alpha\text{-}GeW_9O_{34}]^{10-}$ precursor. Three Fe^{3+} ions in a Fe_3 cluster occupy the vacant sites of the $[B\text{-}\alpha\text{-}GeW_9O_{34}]^{10-}$ subunit in a triangle motif linked together by O atoms. Each Fe center shows an octahedral geometry. The octahedral $Fe1^{3+}$ cation is defined by O atoms (O31, O32 and O33) from the $[B\text{-}\alpha\text{-}GeW_9O_{34}]^{10-}$ subunit [Fe–O: 1.967(14)–2.126(15) Å] and three O atoms (O70, O71, O73) from the $[\alpha\text{-}GeW_6O_{26}]^{12-}$ fragment [Fe–O: 1.886(16)–2.095(13) Å] (Fig. 2b). The coordination environment of the $Fe2^{3+}$ cation is similar to that of the $Fe1^{3+}$ cation and the Fe–O distances are in the range of 1.921(14)–2.139(13) Å. However, the coordination environment of the $Fe3^{3+}$ cation is somewhat different from those of $Fe1^{3+}$ and $Fe2^{3+}$ cations. Three O atoms (O29, O30, O31) from $[B\text{-}\alpha\text{-}GeW_9O_{34}]^{10-}$ [Fe–O: 1.981(15)–2.179(16) Å], two O atoms (O72, O73) from the $[\alpha\text{-}GeW_6O_{26}]^{12-}$ fragment [Fe–O: 2.071(15)–2.103(15) Å] and a water ligand (O93) [Fe–O: 2.014(17) Å] constitute the octahedron. The coordination modes of $Fe4^{3+}$, $Fe5^{3+}$ and $Fe6^{3+}$ cations are similar to those of $Fe1^{3+}$, $Fe2^{3+}$ and $Fe3^{3+}$ cations (Fig. S12†). Even though this double sandwich iron-substituted GT has been reported by our lab in 2009,[26] it is noteworthy that two different aspects should be pointed out: (a) two double sandwich structural units in **2** are interconnected with each other *via* two $K1^{+}$ cations, giving rise to a ring-like assembly, in which the $K1^{+}$ cations exhibit the distorted eight-coordinate square antiprismatic configuration with K–O distances of 2.75(4)–3.027(18) Å (Fig. 2c); (b) two en molecules are anchored in the ring-like assembly (Fig. 2d).

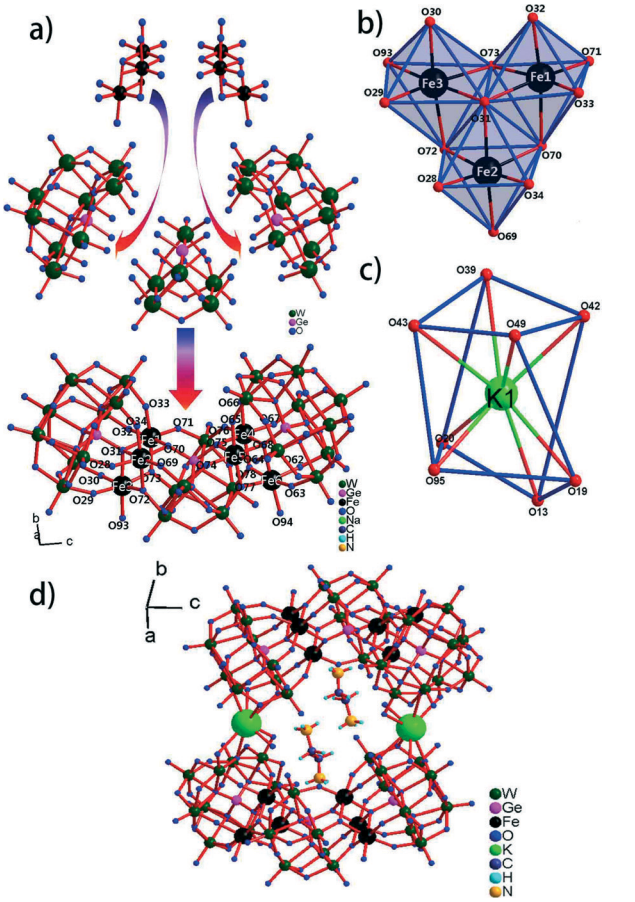

Fig. 2 (a) Ball-and-stick view of the double sandwich cluster in **2**. (b) The six-coordinate octahedral geometries of Fe1, Fe2 and Fe3 cations. (c) The distorted eight-coordinate square antiprismatic configuration of the $K1^{+}$ cation. (d) The ring-like assembly formed by two double sandwich clusters connected *via* two $K1^{+}$ cations.

IR spectra

The IR spectrum of **1** exhibits the characteristic $\nu(Ge\text{–}O_a)$, terminal $\nu(W\text{–}O_t)$, corner-sharing $\nu(W\text{–}O_b)$ and edge-sharing $\nu(W\text{–}O_c)$ asymmetrical vibration patterns derived from Keggin-type GT frameworks (Fig. S1†).[37] The bands at 938, 869, 788 and 651 cm^{-1} can be attributed to $\nu(W\text{–}O_t)$, $\nu(Ge\text{–}O_a)$, $\nu(W\text{–}O_b)$ and $\nu(W\text{–}O_c)$, respectively. Furthermore, the broad vibration band at 3443 cm^{-1} can be regarded as a feature of lattice water molecules and coordinate water molecules.

The resonances at 3124 and 2927 cm^{-1} are assigned to the $\nu(NH_2)$ and $\nu(CH_2)$ stretching vibration, whereas the signals at 1620 and 1492 cm^{-1} correspond to the bending vibration of en ligands. In the IR spectrum of **2** (Fig. S2†), the peaks at 945, 869, 784 and 682 cm^{-1} can be assigned to $\nu(W–O_t)$, $\nu(Ge–O_a)$, $\nu(W–O_b)$, and $\nu(W–O_c)$, respectively. The broad peaks at 3451 cm^{-1} are attributed to the stretching and bending modes of lattice and coordinate water molecules. The pattern of peaks in 3125 and 2927 cm^{-1} results from the $\nu(NH_2)$ and $\nu(CH_2)$ stretching vibration, while the bending vibrations of en ligands are observed at 1617 and 1507 cm^{-1}. In short, the results of the IR spectra are consistent with the single-crystal structural analyses.

TG analyses

The TG behaviors of **1** and **2** were examined on pure crystalline samples under a flowing air atmosphere with a heating rate of 10 °C min^{-1} in the range of 25–800 °C so as to characterize their thermal stability (Fig. S13 and S14†). The TG curve of **1** indicates that the weight loss procedure can be divided into two steps. The first weight loss of 10.47% from 30 to 561 °C corresponds to the release of forty-two lattice water molecules, thirteen diprotonated en molecules and the dehydration of one proton (calcd. 9.64%). The second weight loss of 1.22% between 635 and 800 °C is assigned to the removal of twelve water ligands (calcd. 1.17%). For **2**, the TG data show an initial loss of 9.25% (calcd. 9.37%) from 30 to 529 °C, attributable to the loss of eleven lattice water molecules and six diprotonated en molecules. The second weight loss of 1.07% (calcd. 0.63%) between 561 and 800 °C corresponds to the loss of two water ligands and the dehydration of one proton. These above observations indicate that the experimental values are in good agreement with the structural determination of **1** and **2**.

Magnetic properties

The solid-state direct-current magnetic susceptibilities of **1** and **2** have been measured on their polycrystalline samples at 2–300 K. The magnetic data for **1** are plotted in Fig. 3a in the form of χ_m, $\chi_m T$ and χ_m^{-1} *versus T*. In the χ_m *vs. T* plot of **1**, the χ_m value slowly increases from 0.097 cm^3 mol^{-1} at 300 K to 0.378 cm^3 mol^{-1} at 65 K and then exponentially to the maximum of 2.138 cm^3 mol^{-1} at 3 K, and followed by a decrease to 2.027 cm^3 mol^{-1} at 2 K. In the $\chi_m T$ *vs. T* plot of **1**, the $\chi_m T$ value of 28.3 cm^3 K mol^{-1} at 300 K is slightly higher than the sum (26.78 cm^3 K mol^{-1})[38] of the contribution attributable to six isolated Sm^{III} cations in the $^6H_{5/2}$ group state (J = 5/2, g = 2/7) and six non-interacting Fe^{III} atoms considering g = 2 per formula unit. When the temperature is lowered, the $\chi_m T$ value gradually decreases to the value of 4.10 cm^3 K mol^{-1} at 2 K. This behavior reveals the occurrence of anti-ferromagnetic interactions with {Fe–(μ_3-O)$_3$–Sm} clusters or/and the depopulation of the higher energy Kramers doublets. The $^6H_{5/2}$ ground state for the free Sm^{III} ion in the crystal field is split into six states by spin–orbit coupling, and

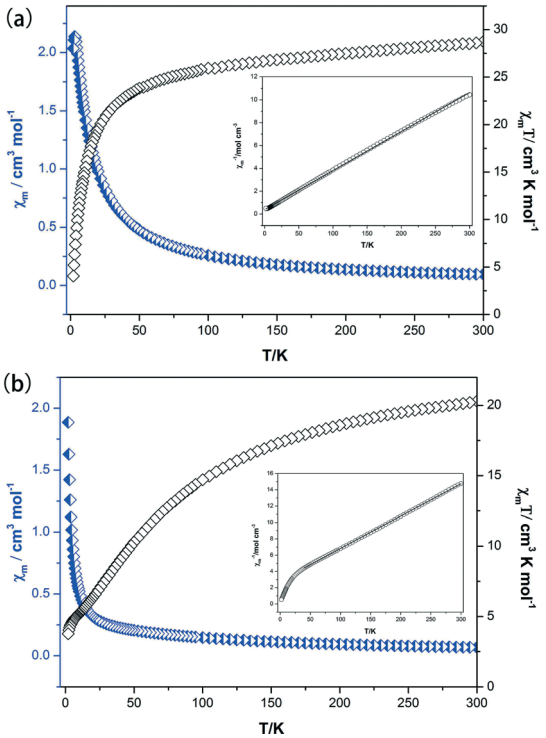

Fig. 3 Temperature dependence of χ_m and $\chi_m T$ values and temperature dependence of reciprocal magnetic susceptibility χ_m^{-1} (inset) for **1** (a) and **2** (b).

the spin–orbit coupling parameter is 1200 cm^{-1}, so the crystal field effect and the possible thermal population of the high energy states should be considered for **1**.[39] The χ^{-1} *vs. T* plot is well fitted with the Curie–Weiss law [$\chi_m = C/(T - \theta)$] in the whole temperature range, resulting in C = 29.25 cm^3 K mol^{-1} and θ = −11.12 K. The negative Weiss temperature further suggests the presence of antiferromagnetic interactions in **1**.

In the case of **2**, the experimental data plotted as χ_m, $\chi_m T$ and χ_m^{-1} *versus T* are shown in Fig. 3b. The χ_m slowly increases from 0.068 cm^3 mol^{-1} at 300 K to 0.261 cm^3 mol^{-1} at 28 K, then exponentially to a maximum of 1.886 cm^3 mol^{-1} at 2 K. The $\chi_m T$ value of 20.3 cm^3 K mol^{-1} at 300 K is significantly much lower than the theoretical value (26.25 cm^3 K mol^{-1}) for six non-interacting Fe^{III} (S = 5/2) with g = 2.00. Upon cooling, the $\chi_m T$ value decreases steadily to 3.7 cm^3 K mol^{-1} at 2 K. This suggests the presence of antiferromagnetic exchange interactions within Fe^{3+} centers. Between 40 and 300 K, the magnetic susceptibility data are well described by the Curie–Weiss expression with Curie constant C = 25.64 cm^3 K mol^{-1} and Weiss constant θ = −73.26 K. This result is fully consistent with the conclusion reported by Yang *et al.* in 2009.[26] As a matter of fact, the antiferromagnetic exchange interactions of the multi-Fe^{III} substituted POMs have been already encountered in previous studies.[22,34] For example, in 2005, Kortz *et al.* discovered a novel Knoth-type hexa-Fe^{III} substituted GT $[Fe_6(OH)_3(A\text{-}\alpha\text{-}GeW_9O_{34}(OH)_3)_2]^{11-}$ and quantificationally investigated its antiferromagnetic behavior.[34] In 2007, Kortz *et al.* reported two antiferromagnetic

di-Fe^{III} and tetra-Fe^{III} sandwiched GTs $[K(H_2O)(\beta\text{-}Fe_2GeW_{10}O_{37}(OH))(\gamma\text{-}GeW_{10}O_{36})]^{12-}$ and $[\{\beta\text{-}Fe_2GeW_{10}O_{37}(OH)_2\}_2]^{12-}$.[22]

Conclusions

In summary, a hexameric Fe–Sm heterometallic GT **1** and a hexa-Fe substituted GT **2** containing di-, tri- or hexavacant Keggin POM fragments have been synthesized and structurally characterized using elemental analyses, IR spectra, PXRD, TG analyses and single-crystal X-ray diffraction. Adjacent hexameric aggregates in **1** are interconnected with each other *via* two $K3^+$ cations, giving rise to the 1-D chain architecture. The divacant $[\alpha\text{-}GeW_{10}O_{38}]^{12-}$ fragment is first observed in the structure of **1**. Notably, **1** is the first heterometallic hexameric GT consisting of six $\{Fe\text{–}(\mu_3\text{-}O)_3\text{–}Sm\}$ bridges, while two double sandwich-type fragments in **2** are connected together through two K^+ cations forming hexameric GT units. The magnetic studies of **1** and **2** show the presence of antiferromagnetic interactions in the two compounds. In the following work, we are aiming at exploring multi-Fe–Ln substituted GTs by using the $[A\text{-}\alpha\text{-}GeW_9O_{34}]^{10-}$ precursor, Fe^{2+}/Fe^{3+} and other Ln materials. By using appropriate TM ions and Ln cations, we hope to obtain some TM–Ln substituted POMs with tunable properties and functionalities.

Acknowledgements

This work was supported by the NNSF of China (nos. 91122028 21221001, 50872133, 21101055), the NNSF for Distinguished Young Scholars of China (no. 20725101), and the 973 program (nos. 2014CB932101 and 2011CB932504).

References

1 J. D. Compain, P. Mialane, A. Dolbecq, I. M. Mbomekallé, J. Marrot, F. Sécheresse, E. Riviere, G. Rogez and W. Wernsdorfer, *Angew. Chem., Int. Ed.*, 2009, **48**, 3077.
2 C. Y. Duan, M. L. Wei, D. Guo, C. He and Q. J. Meng, *J. Am. Chem. Soc.*, 2010, **132**, 3321.
3 C. Y. Sun, S. X. Liu, D. D. Liang, K. Z. Shao, Y. H. Ren and Z. M. Su, *J. Am. Chem. Soc.*, 2009, **131**, 1883.
4 Z. M. Zhang, S. Yao, Y. G. Li, Y. H. Wang, Y. F. Qi and E. B. Wang, *Chem. Commun.*, 2008, 1650.
5 S. T. Zheng, J. Zhang, J. M. C. Juan, D. Q. Yuan and G. Y. Yang, *Angew. Chem., Int. Ed.*, 2009, **48**, 7176.
6 J. W. Zhao, C. M. Wang, J. Zhang, S. T. Zheng and G. Y. Yang, *Chem.–Eur. J.*, 2008, **14**, 9223.
7 D. J. Guo, S. J. Fu, W. Tan and Z. D. Dai, *J. Mater. Chem.*, 2010, **20**, 10159.
8 J. W. Zhao, Q. X. Han, D. Y. Shi, L. J. Chen, P. T. Ma, J. P. Wang and J. Y. Niu, *J. Solid State Chem.*, 2011, **184**, 2756.
9 C. L. Hill, *Chem. Rev.*, 1998, **98**, 1.
10 J. M. Clemente-Juan and E. Coronado, *Coord. Chem. Rev.*, 1999, **193–195**, 361.
11 D. L. Long, E. Burkholder and L. Cronin, *Chem. Soc. Rev.*, 2007, **36**, 105.
12 A. Proust, R. Thouvenot and P. Gouzerh, *Chem. Commun.*, 2008, 1837.
13 (*a*) U. Kortza, A. Müller, J. V. Slagerenc, J. Schnacke, N. S. Dalalf and M. Dressel, *Coord. Chem. Rev.*, 2009, **253**, 2315; (*b*) A. Dolbecq, E. Dumas, C. R. Mayer and P. Mialane, *Chem. Rev.*, 2010, **110**, 6009.
14 (*a*) S.-T. Zheng, D.-Q. Yuan, H.-P. Jia, J. Zhang and G.-Y. Yang, *Chem. Commun.*, 2007, 1858; (*b*) J.-W. Zhao, H.-P. Jia, J. Zhang, S.-T. Zheng and G.-Y. Yang, *Chem.–Eur. J.*, 2007, **13**, 10030; (*c*) S.-T. Zheng, M.-H. Wang and G.-Y. Yang, *Inorg. Chem.*, 2007, **46**, 9503; (*d*) J.-W. Zhao, B. Li, S.-T. Zheng and G.-Y. Yang, *Cryst. Growth Des.*, 2007, **7**, 2658.
15 S.-T. Zheng and G.-Y. Yang, *Chem. Soc. Rev.*, 2012, **41**, 7623.
16 B. Botar, Y. V. Geletii, P. Kögerler, D. G. Musaev, K. Morokuma, I. A. Weinstock and C. L. Hill, *J. Am. Chem. Soc.*, 2006, **128**, 11268.
17 C. T. Kressge, M. E. Leonowicz, W. J. Roth, J. C. Vartuni and J. S. Beck, *Nature*, 1992, **359**, 710.
18 (*a*) B. S. Bassil, S. Nellutla, U. Kortz, A. C. Stowe, J. van Tol, N. S. Dalal, B. Keita and L. Nadjo, *Inorg. Chem.*, 2005, **44**, 2659; (*b*) U. Kortz, S. Nellutla, A. C. Stowe, S. N. Dalal, U. Rauwald, W. Danquah and D. Ravot, *Inorg. Chem.*, 2004, **43**, 2308; (*c*) U. Kortz, S. Nellutla, A. C. Stowe, N. S. Dalal, J. van Tol and B. S. Bassil, *Inorg. Chem.*, 2004, **43**, 144; (*d*) A. C. Stowe, S. Nellutla, N. S. Dalal and U. Kortz, *Eur. J. Inorg. Chem.*, 2004, 3792; (*e*) A. J. Tasiopoulos, A. Vinslava, W. Wernsdorfer, K. A. Abboud and G. Christou, *Angew. Chem., Int. Ed.*, 2004, **43**, 2117.
19 (*a*) M. T. Pope, *Heteropoly and Isopoly Oxometalates*, Springer-Verlag, Berlin, 1983; (*b*) R. Contant and G. Hervé, *Inorg. Chem.*, 2002, **22**, 63.
20 (*a*) O. Sato, *Acc. Chem. Res.*, 2003, **36**, 692; (*b*) L. Ouahab, *Coord. Chem. Rev.*, 1998, **178**, 1501.
21 (*a*) B. Botar, Y. V. Geletii, P. Kögerler, D. G. Musaev, K. Morokuma, I. A. Weinstock and C. L. Hill, *J. Am. Chem. Soc.*, 2006, **128**, 11268; (*b*) B. Botar, P. Kögerler and C. L. Hill, *Inorg. Chem.*, 2007, **46**, 5398.
22 N. H. Nsouli, S. S. Mal, M. H. Dickman, U. Kortz, B. Keita, L. Nadjo and J. M. Clemente-Juan, *Inorg. Chem.*, 2007, **46**, 8763.
23 C. P. Pradeep, D. L. Long, P. Kögerler and L. Cronin, *Chem. Commun.*, 2007, 4254.
24 C. Pichon, A. Dolbecq, P. Mialane, J. Marrot, E. Rivière and F. Sécheresse, *Dalton Trans.*, 2008, 71.
25 A. Dolbecq, J. D. Compain, P. Mialane, J. Marrot, E. Rivière and F. Sécheresse, *Inorg. Chem.*, 2008, **47**, 3371.
26 B. Li, J.-W. Zhao, S.-T. Zheng and G.-Y. Yang, *Inorg. Chem. Commun.*, 2009, **12**, 69.
27 S. W. Lin, W. L. Liu, Y. G. Li, Q. Wu, E. B. Wang and Z. M. Zhang, *Dalton Trans.*, 2010, **39**, 1740.
28 (*a*) X. K. Fang and P. Kögerler, *Chem. Commun.*, 2008, 3396; (*b*) X. K. Fang and P. Kögerler, *Angew. Chem., Int. Ed.*, 2008, **47**, 8123.
29 B. Nohra, P. Mialane, A. Dolbecq, E. Rivière, J. Marrot and F. Sécheresse, *Chem. Commun.*, 2009, 2703.

30 (*a*) W. L. Chen, Y. G. Li, Y. H. Wang and E. B. Wang, *Eur. J. Inorg. Chem.*, 2007, 2216; (*b*) Z. M. Zhang, Y. G. Li, W. L. Chen, E. B. Wang and X. L. Wang, *Inorg. Chem. Commun.*, 2008, **11**, 879; (*c*) W. L. Chen, Y. G. Li, Y. H. Wang, E. B. Wang and Z. M. Zhang, *Dalton Trans.*, 2008, 865.

31 (*a*) J. P. Wang, Q. X. Yan, X. D. Du and J. Y. Niu, *J. Cluster Sci.*, 2008, **19**, 491; (*b*) H. Pang, C. Zhang, D. Shi and Y. Chen, *Cryst. Growth Des.*, 2008, **8**, 4476.

32 (*a*) C. D. Wu, C. Z. Lu, H. H. Zhuang and J. S. Huang, *J. Am. Chem. Soc.*, 2002, **124**, 3836; (*b*) P. Mialane, A. Dolbecq, E. Rivière, J. Marrot and F. Sécheresse, *Eur. J. Inorg. Chem.*, 2004, 33; (*c*) J. W. Zhao, D. Y. Shi, L. J. Chen, Y. Z. Li, P. T. Ma, J. P. Wang and J. Y. Niu, *Dalton Trans.*, 2012, **41**, 10740.

33 Z. M. Zhang, Y. G. Li, S. Yao and E. B. Wang, *Dalton Trans.*, 2011, **40**, 6475.

34 L. H. Bi, U. Kortz, S. Nellutla, A. C. Stowe, J. van Tol, N. S. Dalal, B. Keita and L. Nadjo, *Inorg. Chem.*, 2005, **44**, 896.

35 (*a*) G. M. Sheldrick, *SHELXL97, Program for Crystal Structure Solution*, University of Göttingen, Germany, 1997; (*b*) G. M. Sheldrick, *SHELXL 97, Program for Crystal Structure Refinement*, University of Göttingen, Germany, 1997.

36 (*a*) I. D. Brown and D. Altermatt, *Acta Crystallogr., Sect. B: Struct. Sci.*, 1985, **41**, 244; (*b*) H. H. Thorp, *Inorg. Chem.*, 1992, **31**, 1585.

37 L. H. Bi, U. Kortz, B. Keita and L. Nadjo, *Dalton Trans.*, 2004, 3184.

38 C. Benelli and D. Gatteschi, *Chem. Rev.*, 2002, **102**, 2369.

39 (*a*) J. Niu, K. Wang, H. Chen, J. Zhao, P. Ma, J. Wang, M. Li, Y. Bai and D. Dang, *Cryst. Growth Des.*, 2009, **9**, 4362; (*b*) M. Andruh, E. Bakalbassis, O. Kahn, J. C. Trombe and P. Porcher, *Inorg. Chem.*, 1993, **32**, 1616.